A 15–40-GHz Frequency Reconfigurable RF MEMS Phase Shifter

Mehmet Unlu, *Member, IEEE*, Simsek Demir, *Member, IEEE*, and Tayfun Akin, *Member, IEEE*

***Abstract*—This paper presents a novel frequency reconfigurable phase shifter using the RF microelectromechanical systems (MEMS) technology. The phase shifter is based on the triple-stub circuit topology composed of three stubs that are connected by two transmission lines that are all implemented as distributed MEMS transmission lines. The insertion phase of the circuit is controlled by changing the electrical lengths of the stubs and the connecting transmission lines, while having ideally zero reflection coefficient at all times. The phase shifter has theoretically no specific limits on the frequency; in other words, it can be reconfigured to work at *any* frequency between 15–40 GHz, with adjustable phase steps, while providing a constant time delay within a 2%–3% instantaneous bandwidth around any selected center frequency in the above-mentioned band. The phase shifter is fabricated monolithically using a surface micromachining process on a quartz substrate and occupies 10.8 mm $\times$ 5.9 mm. Measurement results show that the phase shifter has average phase error of 1.6°, 3.7°, and 4.7°, average insertion loss of 3.1, 5, and 8.2 dB and average return loss of 19.3, 15.8, and 13.7 dB at 15, 30, and 40 GHz, respectively. To the best of our knowledge, this paper demonstrates the first phase shifter in the literature that can work at any given frequency in a targeted band with adjustable phase steps.**

***Index Terms*—Microelectromechanical systems (MEMS), periodic structures, phase shifters, reconfigurable circuits, RF MEMS.**

I. Introduction

PHASE shifters are crucial components in a number of applications that include communications, high-precision instrumentation, and radars. Phase shifters can be categorized in two main groups in terms of the application requirements with respect to frequency: the constant phase and linear phase type phase shifters. The constant phase types target providing a constant phase difference in a wide instantaneous bandwidth [1]–[3], whereas the linear phase types provide linearly increasing phase difference, corresponding to true time delay (TTD). Several efforts have been made on both types of phase shifters in order to satisfy the increasing requirements of the modern RF systems that demand wide bandwidth and reconfigurable operation.

Reconfigurable phase shifters have been implemented using several different methods including ferroelectric, photonic, and liquid-crystal technologies [4]–[8]. The RF microelectromechanical systems (MEMS) technology has also been offering low-loss and low-cost TTD phase shifters in the last decade [9]–[16], which can be grouped as the switched network [9]–[12] and distributed MEMS transmission line (DMTL) [13]–[16] phase shifters. The switched network MEMS phase shifters present very good performance up to 40 GHz with a maximum of 4-bit resolution, while DMTL phase shifters approach 110 GHz with excellent insertion loss and linearity performances with the similar resolutions. However, although their presented performance is impressive, the desired phase shift can only be achieved at a single frequency, and as a result, separate phase shifters must be used for each frequency of interest. Furthermore, these phase shifters are designed for a specific phase step, and there are no TTD type phase shifters reported with reconfigurable phase steps.

A novel method to implement phase shifters is reported recently [20], which is based on the triple-stub topology. This topology is very well known for its ability to make impedance transformation to any given impedance. Reconfigurable triple-stub impedance tuners are reported that use RF MEMS technology [17]–[19]; however, triple-stub topology has not been reported for any applications other than impedance tuning.

This paper presents a novel wideband frequency reconfigurable RF MEMS phase shifter that employs the triple-stub circuit topology. The triple-stub phase shifter has three stubs and two connecting transmission lines, all of which are implemented as DMTLs. The insertion phase of the phase shifter is controlled by changing the electrical lengths of the stubs and connecting transmission lines. The presented phase shifter is capable of providing constant time delay within 2%–3% bandwidth *at any frequency between 15–40 GHz*, while it can be operated with adjustable phase steps at each selected frequency. *To our knowledge, this is the first time presentation of a frequency reconfigurable phase shifter with adjustable phase steps*. The proposed phase shifter may be a strong candidate and can replace multiple phase shifters in multi-frequency or wideband RF front-ends and phased arrays.

II. Phase-Shifter Design

Fig. 1 shows the schematic of the proposed phase shifter, which is based on the triple-stub circuit topology. The phase shifter is composed of stubs and connecting transmission lines, and the desired insertion phase is achieved by changing the electrical lengths of all of these components, as shown in Fig. 1(a).

Manuscript received December 13, 2012; revised May 18, 2013; accepted May 21, 2013. Date of publication July 17, 2013; date of current version August 02, 2013. This work was supported by The Scientific and Technical Research Council of Turkey (TUBITAK-EEEAG-104E048) and the Turkish State Planning Organization (DPT).

M. Unlu is with the Electronics and Communication Engineering Department, Yildirim Beyazit University, Ankara 06030, Turkey (e-mail: munlu@ybu.edu.tr).

S. Demir and T. Akin are with the Department of Electrical and Electronics Engineering, Middle East Technical University (METU), Ankara 06531, Turkey.

Color versions of one or more of the figures in this paper are available online at http://ieeexplore.ieee.org.

Digital Object Identifier 10.1109/TMTT.2013.2271995

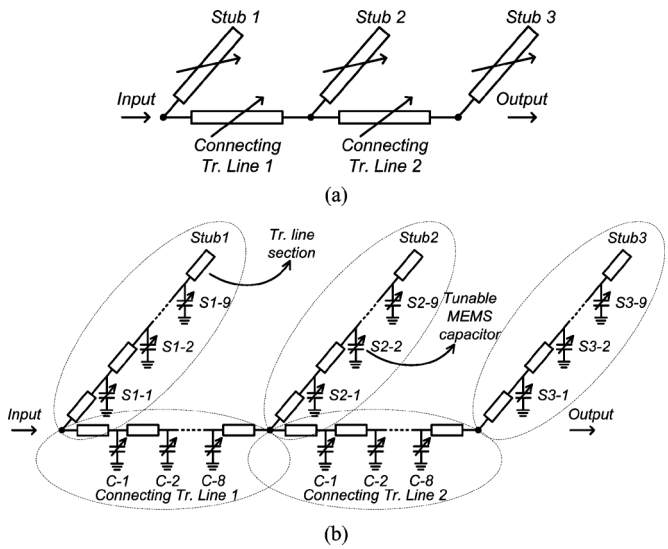

Fig. 1. Schematic of the proposed triple-stub based phase shifter. (a) Simplified representation with tunable electrical length transmission lines. (b) Representation with DMTLs.

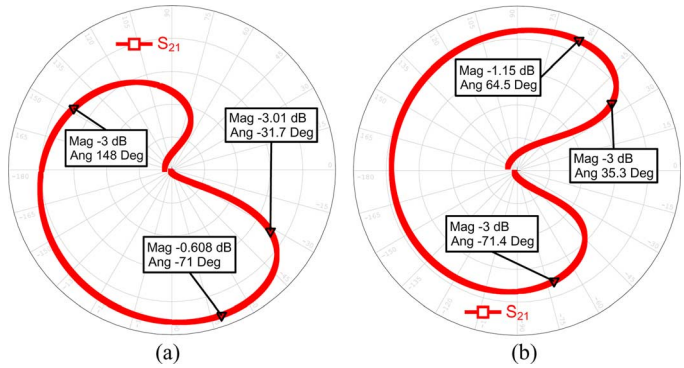

Fig. 2. Insertion phase range of triple-stub circuit topology with acceptable insertion loss for different connecting transmission line lengths. (a) 0.1λ. (b) 0.4λ.

The theory behind phase shifting using the triple-stub circuit topology was previously introduced by the authors [20], where the analytical and numerical solutions, operation principles, and experimental results *for fixed electrical lengths* were presented as the proof of concept. Here, in this paper, we concentrate on a real life application of the idea and present a wideband frequency reconfigurable phase shifter based on the triple-stub circuit topology, where the electrical lengths of the stubs and connecting transmission lines are tuned by means of periodically placed tunable MEMS capacitors, or in the more commonly used name, DMTLs [see Fig. 1(b)]. The choice of the triple-stub circuit topology grants the ability of changing the insertion phase in the whole 0°–360° range while keeping the reflection coefficient theoretically zero at all times, which makes it very suitable for a phase shifter.

The design of the phase shifter starts with determining the required electrical length ranges of the stubs and connecting transmission lines for the proper operation of the phase shifter using the analytical formulation given in [20]. The next step is to design the DMTLs for stubs and connecting transmission lines that satisfy the requirements coming from the first step. Finally, the overall design of the phase shifter will be presented.

Before discussing the details of the design, one point about the design methodology should be clarified. The proposed reconfigurable phase shifter has been designed for operating *at any given frequency* within the whole 15–40-GHz band. However, the calculations were made considering the lowest frequency of the band, which is 15 GHz. This is because the change in the electrical lengths of the stubs and connecting transmission lines should be long enough at this frequency so as to assure the proper operation of the phase shifter. On the other hand, the electrical lengths at any frequency greater than 15 GHz are automatically longer, which guarantees the operation of the phase shifter at these frequencies. The price paid here is the decrease in the resolution of the phase shifter as the operation frequency is increased, and the design was checked for sample frequencies to ensure its operation all over the 15–40-GHz band.

A. Determination of the Design Requirements

It was stated in [20] that in the presence of transmission lines losses, there exists a range of insertion phases that the triple-stub circuit topology can provide with an acceptable insertion loss for each electrical length of the connecting transmission lines. This range can be adjusted by changing the electrical length of the connecting transmission lines. It is found using the formulation presented in [20] that an insertion phase between 35°–325° can be easily obtained by selecting the electrical length of the connecting transmission lines between 0.1λ and 0.4λ at 15 GHz, as presented in Fig. 2. However, in order to attain an insertion phase between 0°–35° or 330°–360°, the electrical length of the connecting transmission lines should be tuned accurately in the $0-0.1\lambda$ and $0.4\lambda-0.5\lambda$ ranges, respectively. Thus, the DMTL design that will be used for connecting transmission lines should be able to change the insertion phase of the interconnection line between $-150°$ and $-215°$ with 5° steps. It can be easily shown that 5° insertion phase resolution for the connection transmission lines results in a 2° insertion phase resolution of the phase shifter.

The electrical lengths of the stubs should also be selected correctly so that they provide the required reflection coefficients for the proper operation of the phase shifter. The formulation presented in [20] necessitates that the electrical lengths of the stubs should be changed in $0-0.5\lambda$, which corresponds to 0°–360° change in the phase of the reflection coefficient. In this case, the phase shifter is able to cover 0°–360° insertion phase range. However, once the electrical lengths of the connecting transmission lines are limited to the aforementioned range, it is found out that the phase shifter can still provide any insertion phase between 0° and 360° if the phases of reflections coefficients of the stubs remain between $-143°$ and 120°. This range is the worst case requirement, and it comes from the second stub. Nevertheless, this range is targeted for the DMTL design of all of the three stubs for the sake of design simplicity. A detailed explanation of the determination of the design requirements can be found in [21].

B. T-Junction Design

The stubs and connecting transmission lines are implemented on coplanar waveguides (CPWs) and CPW T-junctions are necessary at their connection points. The CPW T-junction design is critical in the sense that it must have the same loaded line impedance at all three of its ports. This is because any reflections at these points can significantly disturb the overall insertion phase of the connecting transmission lines, which is critical for the overall phase-shifter design. In addition to that, it also adds an electrical length to the connecting transmission lines, which must be taken into account for the connecting lines.

The CPW T-junction was designed and optimized using HFSS v10 [22], and its operation is verified in AWR Microwave Office (MWO) [23] by comparing it with a T-junction that is made of only ideal transmission lines. The error between the S-parameters of the designed T-junction with that of the ideal model was less than 10^{-7}. The comparison with the ideal model showed that the designed CPW T-junction behaves as a 20°-long transmission line on each side of the connecting transmission lines at 15 GHz, which was taken into account for the design of the connecting transmission lines.

C. DMTL Design for Connecting Transmission Lines

The DMTL design for the connecting transmission lines is a tough design problem since the important parameter is not only the differential phase shift as in standard DMTL phase shifters, but also the electrical length in the up state of the DMTL. The design requirement for the electrical length of the connecting transmission line was that it should stay between $-150°$ and $-215°$; however, since the T-junctions already add $2 \times -20° = -40°$ at both sides, the DTML is designed to work in the $-110°$ and $-175°$ range.

Two types of DMTL unit sections, namely, US-I and US-II, are designed for the connecting transmission lines, which give 5° and 10° differential phase shifts, respectively. The design starts using the DMTL formulation given in [15] and [24], which is followed by the simulations using the circuit model given in Fig. 3. Full-wave EM simulations are then carried out for all unit sections using HFSS version 10. The circuit model parameters (Fig. 3) are finally extracted from HFSS simulations for each unit section for design verification and optimization.

The top view of US-I is given in Fig. 4(a), where dimensions are indicated for all of the unit section designs. Fig. 4(b) presents the 3-D view of US-II. The two metal–air–metal (MAM) capacitors on both sides of the MEMS bridge have some differences from a regular parallel-plate capacitor. They are divided into rectangular bridges by slots in the lateral direction and have a post in the vertical direction so that their height will be immune to the residual stress. In the circuit model, the total bridge and MAM capacitor resistance, R_b, and the resistance due to external resistive bias line, R_{bias}, are both included in order to examine their loss contributions separately. Table I presents the dimensions of DMTL US-I and US-II. Corresponding design parameters are given in Table III in comparison with the parameters that are extracted from the measurements in the following sections.

The MEMS switch that is used in US-I and US-II (as well as US-III, which is used for DMTL design for stubs)

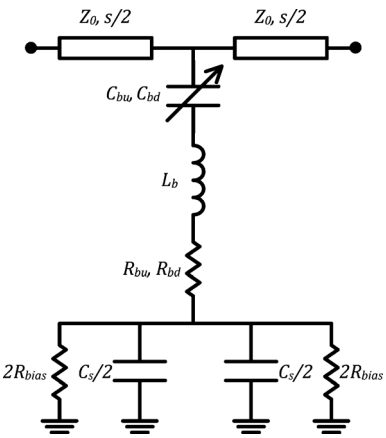

Fig. 3. General schematic of the DMTL unit sections that is used in the phase-shifter design.

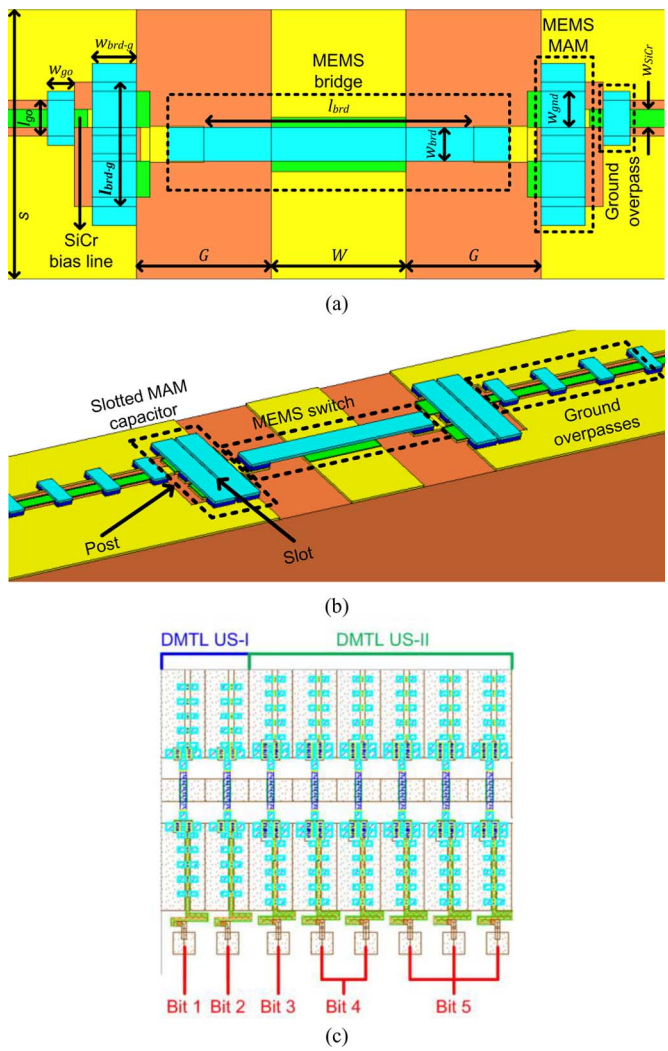

Fig. 4. (a) Top view of DMTL US-I. (b) 3-D view of DMTL US-II. (c) Layout of the DMTL for connecting transmission lines.

is a fixed–fixed beam type, capacitive, shunt switch, and its dimensions are given in Table I. It has a measured up/down capacitance ratio of 7.1 and a measured quality factor of 65 and 48 for up and down states, respectively. These results satisfy the design requirements for all of the unit sections, and are

TABLE I
PHYSICAL DIMENSIONS OF THE DMTL UNIT SECTIONS THAT ARE USED IN THE PHASE-SHIFTER DESIGN

	DMTL US-I	DMTL US-II	DMTL US-III
W	150 μm	150 μm	150 μm
G	150 μm	150 μm	150 μm
l_{brd}	300 μm	300 μm	300 μm
w_{brd}	38 μm	38 μm	38 μm
w_{gnd}	40 μm	40 μm	46 μm
$l_{brd\text{-}g}$	138 μm	138 μm	138 μm
$w_{brd\text{-}g}$	49 μm	2 x 44 μm	4 x 43 μm
w_{go}	30 μm	30 μm	30 μm
l_{go}	40 μm	40 μm	40 μm
w_{SiCr}	20 μm	20 μm	20 μm
s	300 μm	300 μm	210 μm

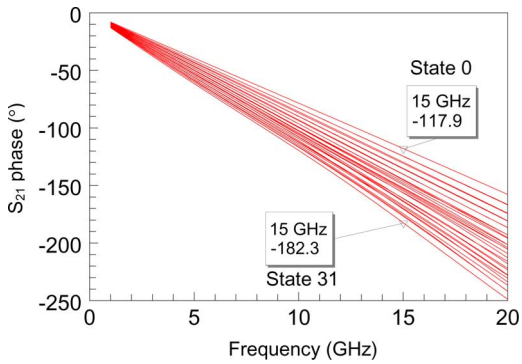

Fig. 5. Simulated unwrapped insertion phase for all 32 states of the DMTL design for the connecting transmission lines.

comparably close to the ones presented in similar structures in the literature [15], [19].

The same DMTL design is used for both connecting transmission lines. These lines are composed of two US-Is and six US-IIs. The connecting transmission line is capable of providing $2 \times 5^\circ + 6 \times 10^\circ = 70^\circ$ differential phase shift, and it is controlled by five control pins, as shown in providing an insertion phase with 5° steps in $2^5 = 32$ states. The layout of the DMTL connecting transmission line is given in Fig. 4(c).

The final simulations of the DMTL for connecting transmission lines are performed by cascading the circuit models (Fig. 3) of all eight unit sections in MWO, and the results are given in Fig. 5. The simulations show that a linear phase response is observed, and the requirements given in Section II-A are satisfied. It should be noted one more time here that the results are presented at the minimum frequency of the band of interest, which is 15 GHz. This is because once the electrical length requirements are satisfied at this frequency, they are automatically satisfied for the rest of the band of interest, as explained previously in the beginning of Section II.

D. DMTL Design for Stubs

According to [20], stubs with different electrical lengths are required for the phase shifter. In the presented reconfigurable phase shifter, a single DMTL is designed that covers the maximum electrical length requirement for all of the three stubs with

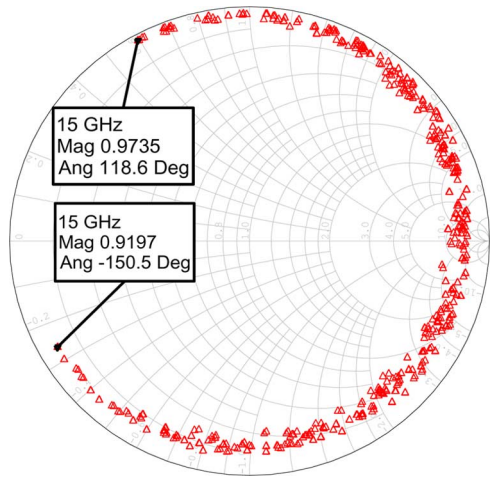

Fig. 6. Simulated S_{11} performance of the DMTL design for the stubs for $2^9 = 512$ states at 15 GHz.

minimum resolution possible. DMTL stubs are expected to provide the reflection coefficients with required phase and a magnitude that is close to 1. Thus, DMTL design for the stubs does not necessarily need to behave like a 50-Ω transmission line as opposed to the DMTL design for the connecting transmission lines.

A third DMTL unit section, US-III, is designed for the stubs using the same methodology explained above. Its physical dimensions are presented in Table I. The design parameters will also be presented in Table III in the following sections.

The overall DMTL design for the stubs is simulated in MWO by cascading nine US-IIIs. The simulation results are given for $2^9 = 512$ states in Fig. 6. It is seen that the required range of electrical length, i.e., the phase of the reflection coefficient, is guaranteed, and the magnitude of the reflection coefficient is close to 1 at all times.

Ground overpasses are used on both sides of the ground plane in order to preserve the continuity of the ground plane of the CPW. Multiple narrow air bridges are used instead of a one-piece overpass that is covering the whole resistive bias line [15]. This is done to reduce the coupling between the ground plane and the resistive bias line, and hence, reducing the loss due to the bias line. As reported in [15], the unit sections with resistive connections to outside under the ground plane have much higher losses compared to that of the ones without the bias lines. Since each of the unit sections on the stubs, as well as most of the unit sections on the connecting transmission lines, have to be controlled independently, a resistive line is needed for each unit section. Thus, the losses due to the resistive bias lines share a major portion of the overall loss of the presented phase shifter.

E. Overall RF MEMS Phase Shifter Design

The final step in the design of the RF MEMS phase shifter is to connect all of the separately designed components and make final simulations in order to verify its operation. Fig. 8 presents the layout of the phase shifter. It has 3×9 control pins for the DMTL stubs and five control pins common to both of the DMTL

TABLE II
SUMMARY OF THE SIMULATION RESULTS OF THE PHASE SHIFTER AT THREE SAMPLE FREQUENCIES WITHIN 15–40-GHz BAND

Freq. (GHz)	No. of States	Resolution (°)	Avg. IL (dB)	Std. Dev. (dB)	Avg. RL (dB)	Std. Dev. (dB)	Avg. Phase Err. (°)	Std. Dev. (°)
15	36	10	2.1	0.7	24	7	0.6	0.8
25	8	45	2.7	0.4	23	8	0.5	0.4
40	8	45	4.4	0.5	19.5	7	11.6	3.2

TABLE III
SIMULATED AND THE MEASURED PARAMETERS OF THE DMTL UNIT SECTIONS THAT ARE USED IN THE PHASE-SHIFTER DESIGN

	DMTL US-I		DMTL US-II		DMTL US-III	
	Sim.	Meas.	Sim.	Meas.	Sim.	Meas.
Z_o (Ω)	96	96	96	96	96	96
$\varepsilon_{r,eff}$	2.36	2.43	2.36	2.43	2.36	2.43
α_{un} (dB/m)[a]	40	38	40	38	40	38
f_{Bragg} (GHz)	73	77	59	62	50	54
Z_{lu} (Ω)	55.9	54.2	52.9	51.6	44.1	39.7
Z_{ld} (Ω)	40.9	42.3	34.5	35.2	23.7	22.3
ϕ_{up} (°)	-14.1	-14.8	-15	-16	-12.6	-13.9
ϕ_{down}(°)	-20	-18.7	-24	-22.9	-25.4	-23.5
$\Delta\phi$	5.9	3.9	9.1	6.9	12.8	9.6
C_{bu} (fF)	46.4	61.5	46.7	62.3	46.3	67.7
C_{bd} (fF)	469.2	439.8	469.2	439.8	469.2	439.8
C_s (fF)	89.5	74.8	147.6	128.6	296.7	232.2
L_b (pH)	30	29.79	30	29.79	30	29.79
R_{bu}/R_{bd} (Ω)	1.6 / 0.15	2 / 0.38	1.6 / 0.15	2 / 0.38	1.6 / 0.15	2 / 0.38
R_{bias} (Ω)	1400	2718	1542	2120	1784	1300

[a]The unloaded CPW losses are reported for 20 GHz.

connecting transmission lines, which make a total of 32 control pins. The layout of the design measures 10750 μm × 5915 μm.

The RF MEMS phase shifter is simulated using MWO by cascading the $ABCD$ parameters of separately designed blocks, which are the T-junctions, DMTLs for the connecting transmission lines, and DMTLs for the stubs. For each insertion phase state, the required electrical lengths of the connecting transmission lines and stubs are determined by the formulation in [20], and the states that give the closest electrical lengths to the required value is selected for that insertion phase state. The values of the calculated electrical lines are also verified by using a special Simplex optimization method where the digital states of all of the DMTLs are used as optimization variables.

The presented design can provide 10°-step operation in an instantaneous bandwidth of 500 MHz at 15 GHz, and this is actually the lower frequency limit of the presented design. It is capable of providing the phase shifter operation *at any selected frequency between 15–40 GHz* while it still preserves the minimum instantaneous bandwidth of 500 MHz. This bandwidth may increase up to 1 GHz depending on the selected center frequency. The only limitation in the operation of the phase shifter is the increasing phase step size as the frequency increases. This is because the insertion phase provided by each unit section increases with frequency, which decreases the phase resolution of the DMTL designs, and as a result, the overall phase step size of the phase shifter increases with frequency.

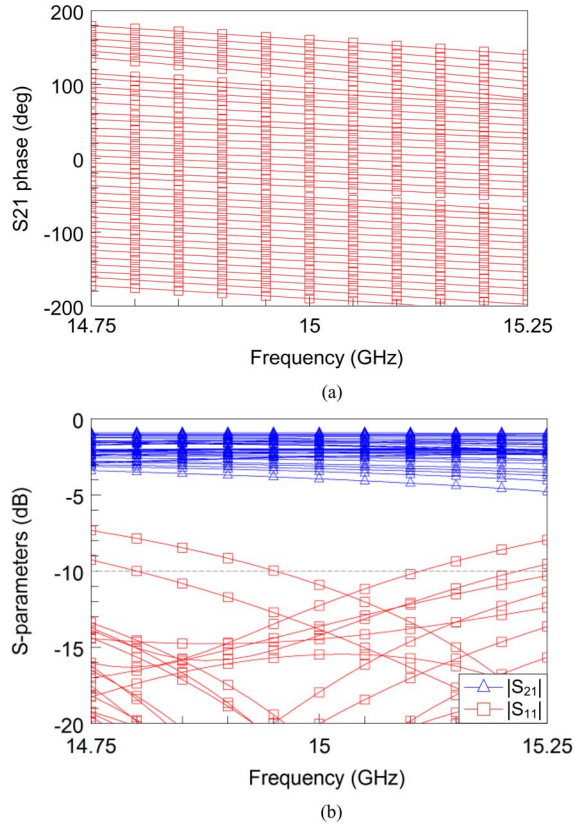

Fig. 7. Simulated performance the RF MEMS phase shifter for 10°-step operation in all 36 states at 15 GHz. (a) Insertion phase. (b) Insertion loss and return loss.

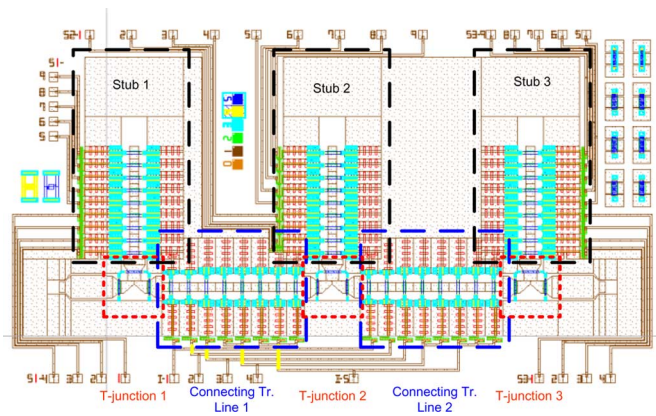

Fig. 8. Final layout of the RF MEMS phase shifter.

The simulations results of the RF MEMS phase shifter are shown in Fig. 7 at 15 GHz, where 0°–360° insertion phase range is covered with 10° steps. Fig. 9 shows the performance of the phase shifter at two selected center frequencies, which are 25 and 40 GHz, when it is set to operate in 45° steps. It should be noted here that Fig. 9(b) shows only half of the instantaneous bandwidth as the phase shifter is set to 40 GHz center frequency in this case. The simulation results are summarized in Table II, which shows that the presented phase shifter can work within the whole targeted frequency band of 15–40 GHz with good performance.

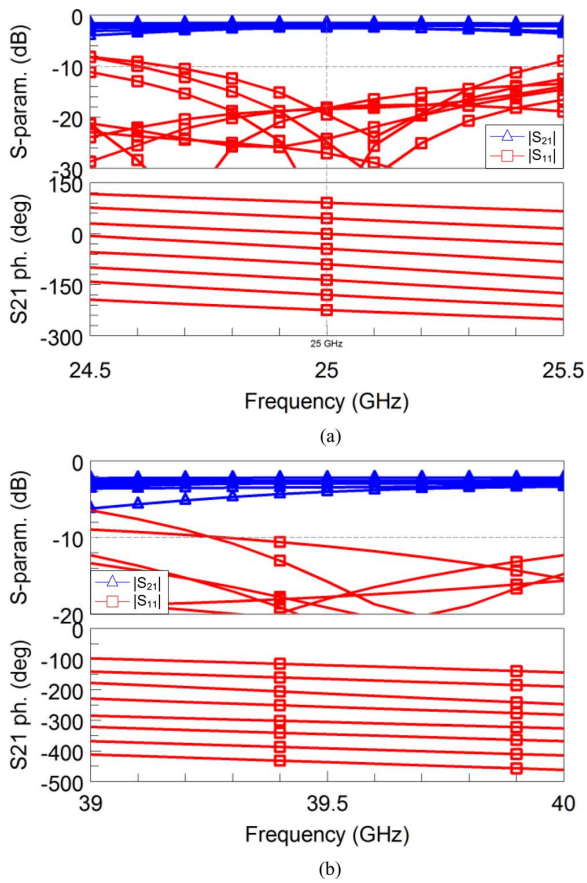

Fig. 9. Performance of the RF MEMS phase shifter for 45°-step operation at two sample frequencies. (a) 25 GHz. (b) 40 GHz.

III. Fabrication

The proposed RF MEMS phase shifter is fabricated using the surface micromachining process developed at the Middle East Technical University (METU) on a 500-μm-thick quartz substrate ($\varepsilon_r = 3.8, \tan\delta = 0.001$). This process, which is detailed in Fig. 10, can be summarized as follows.

1) The SiCr resistive layer (1000 Å) is deposited using RF sputtering and patterned using wet etching as the first step of the process [see Fig. 10(a)]. This layer has a resistivity of 1000 Ω/□.
2) The Ti–Au (100/9000 Å) first metal layer is deposited using dc sputtering and patterned using wet etching [see Fig. 10(a)].
3) The Si_xN_y (3000 Å) isolation layer is deposited using plasma enhanced chemical vapor deposition (PECVD) and patterned using reactive ion etching [see Fig. 10(b)].
4) The polyimide sacrificial layer (2 μm) is deposited using spin coating, patterned using lithography, and cured [see Fig. 10(c)].
5) Au (1.1 μm) is deposited as the structural layer, which is used for forming the MEMS bridges using dc sputtering [see Fig. 10(c)].
6) Au (3.5 μm) is electroplated selectively as the strengthening layer on the anchor points of the RF MEMS switches [see Fig. 10(d)].

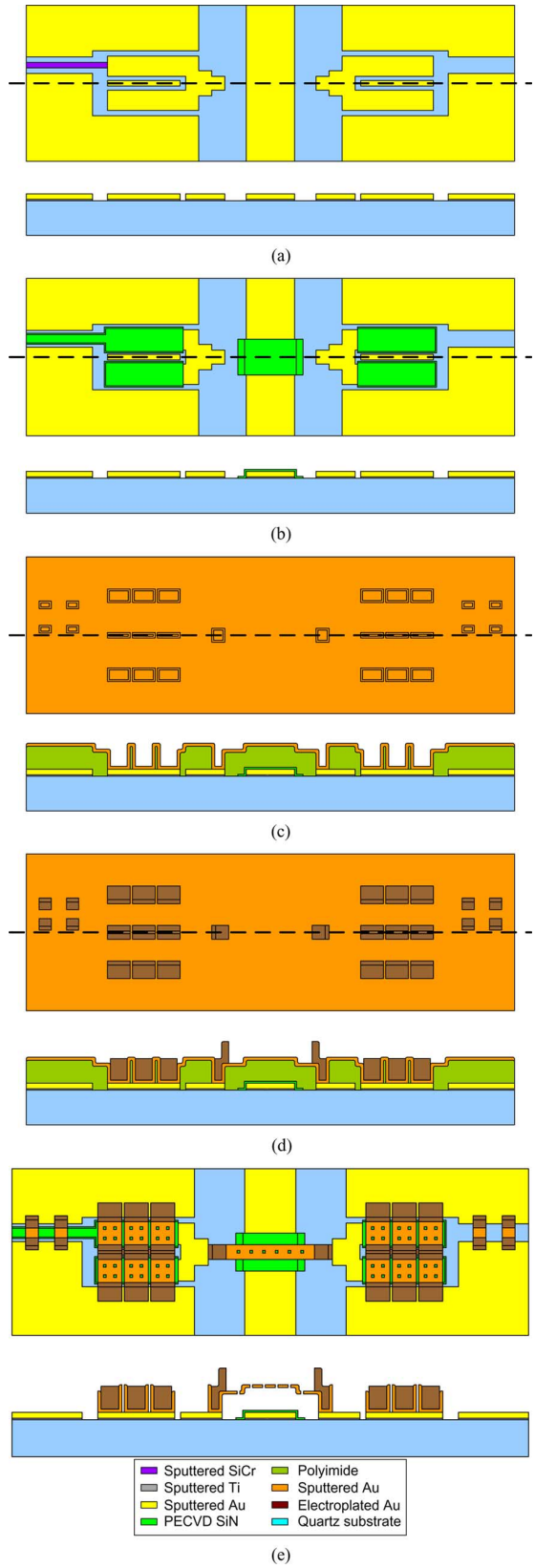

Fig. 10. Process flow of the METU RF MEMS fabrication process that is used for the fabrication of the proposed phase shifters. (a) Resistive and first metal layer deposition and patterning. (b) Isolation layer deposition and patterning. (c) Sacrificial layer deposition and patterning and structural layer deposition. (d) Strengthening layer selective deposition. (e) Structural layer patterning, sacrificial layer etching, and release.

7) The Au structural layer is patterned using wet etching [see Fig. 10(e)].

8) The sacrificial layer is wet etched, and the structures are released using a critical point drying system [see Fig. 10(e)]. Fig. 11 presents the photographs of the fabricated RF MEMS phase shifter and SEM image of one of the 43 MEMS bridges.

IV. Measurement Results

A. Measurement Setup

An automated measurement is needed for the measurements of the fabricated phase shifter since there are 32 control pins, all of which should be controlled simultaneously. For this purpose, a multi-pin MEMS automated measurement setup (MAMS) is designed and implemented. Fig. 12 shows the block diagram of the setup. The setup consists of six main parts, which are: 1) the network analyzer; 2) the probe station; 3) the waveform generator circuit to produce the biasing waveform [bipolar unilevel cycling bias waveform that is used for actuating the MEMS switches, one printed circuit board (PCB)]; 4) the biasing waveform distribution system to direct the waveform to the MEMS switches on the correct time and order (five PCBs); 5) two dc supplies; and 6) the computer to control the whole setup and save the data. The states of the 32 MEMS switches are determined by the computer for each state of the phase shifter. The state data is then sent to the biasing waveform distribution system. The system is composed of four PCBs, each of which controls eight MEMS switches, plus a multiplexer PCB, which controls these four PCBs and distributes the biasing waveform to these PCBs. Detailed information about MAMS can be found in [21].

The fabricated phase shifter is packaged using an integrated circuit package for making the dc connections to the MAMS. CSB03228 ceramic package from Spectrum-Semi is used. The phase shifter is measured using the short-open-load-thru (SOLT) calibration technique in the 10–40-GHz frequency range, and Cascade ACP GSG-150 coplanar probes are used for the RF connections.

The actuation voltage of the MEMS switch, which is used in all three types of DMTL unit sections, is measured as 8 V, and the switch can withstand up to 130 V without breakdown with the price paid for increased dielectric charging. Nevertheless, the phase shifter is measured with 20 V-peak bipolar unilevel waveform that is generated by the waveform generation circuit. The reason for using a waveform with a higher peak voltage is to maximize the contact between the MEMS bridge and dielectric layer, and the switch performance is almost the same for any voltage greater than 20 V. The switching time of the MEMS switch is measured as 8 μs. The measurements show that the switch has a good reliability, and the measured lifetime is 885 h when it is actuated by a bipolar unilevel cycling bias waveform with 1-kHz actuation frequency and 50% duty cycle [25].

During the phase-shifter measurements, more than 40 samples were measured successfully before packaging for a sample set of states under an RF power of up to 0 dBm. The phase-shift measurements were then made at several sample frequencies for hundreds of different phase states on a few samples. None of these samples failed during the tests that took several hours. It is important to note here that for each test, a set of MEMS switches were in the down state for the majority of the test time. The authors expect the dielectric charging of the MEMS switches as the main failure mechanism, but the total test time for any sample, which is in the order of several hours, was not long enough to observe the failure of any of the phase-shifter samples.

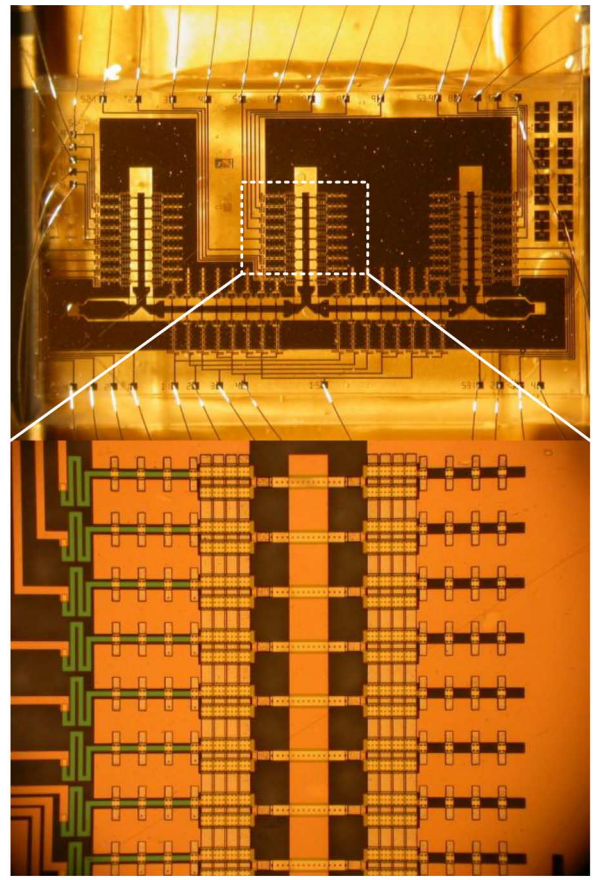

(a)

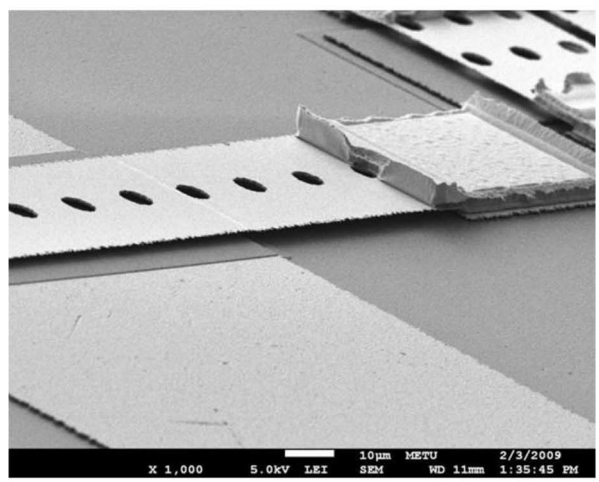

(b)

Fig. 11. (a) Photographs of the fabricated RF MEMS phase shifter. (b) SEM image of the one of the MEMS bridges on the phase shifter.

B. DMTL Parameter Extraction

Each parameter in the circuit model (Fig. 3) is extracted from the measurements of dedicated test structures, which is very

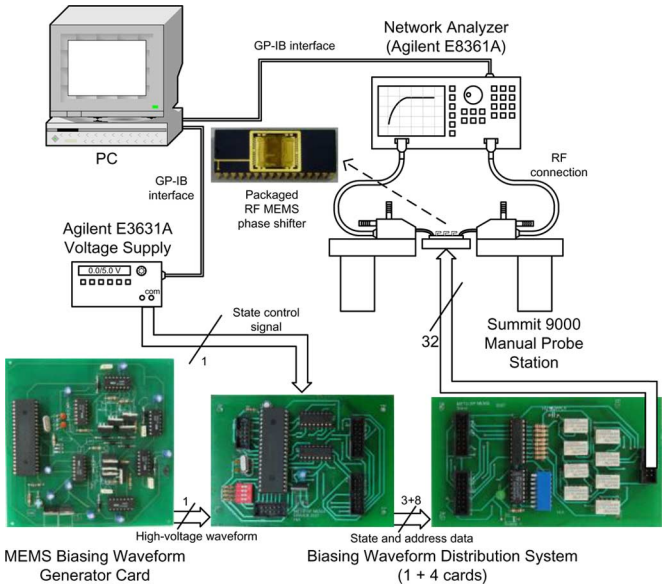

Fig. 12. Block diagram of the MAMS.

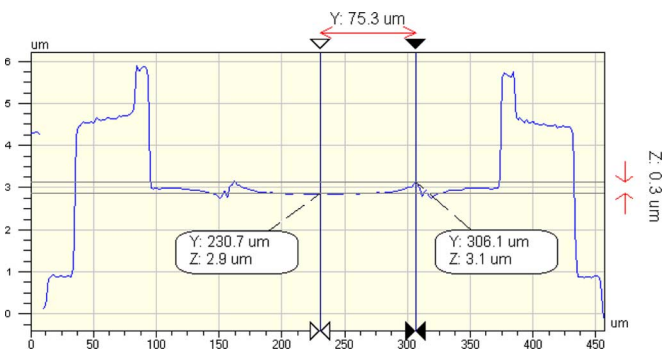

Fig. 13. Optical profilometer measurements of one of the MEMS switches on the fabricated phase shifter. It is clear from the measurements that the MEMS bridge cannot follow the pattern underneath when it passes over the center conductor of the CPW.

critical for the characterization of the fabricated phase shifter. These structures are transmission lines, which physically include and are loaded only by one of the related circuit model parameters. The structures are fabricated on the same wafer with the RF MEMS phase shifter. There are three versions of each test structure for each DMTL type, and the parameters of each DMTL unit section are measured independently. The extracted parameters are presented in Table III.

Table III shows that the measured parameters are mostly close to the simulated ones. The up-state capacitance of the MEMS switch, C_{bu}, is measured to be higher than the simulated one. This is because the MEMS bridges are bent downwards due to the weak step points that occur at the edges of the CPW center conductor. The extracted capacitance calculations show that the MEMS bridge height, i.e., the gap between the MEMS bridge and CPW, is around 2 μm, where it was aimed to be 2.9 μm. This is also verified with optical profilometer measurements that are presented in Fig. 13. The residual stress of the structural layer is actually optimized and measured as low as 40 MPa, which is more than enough to obtain flat MEMS bridges when there

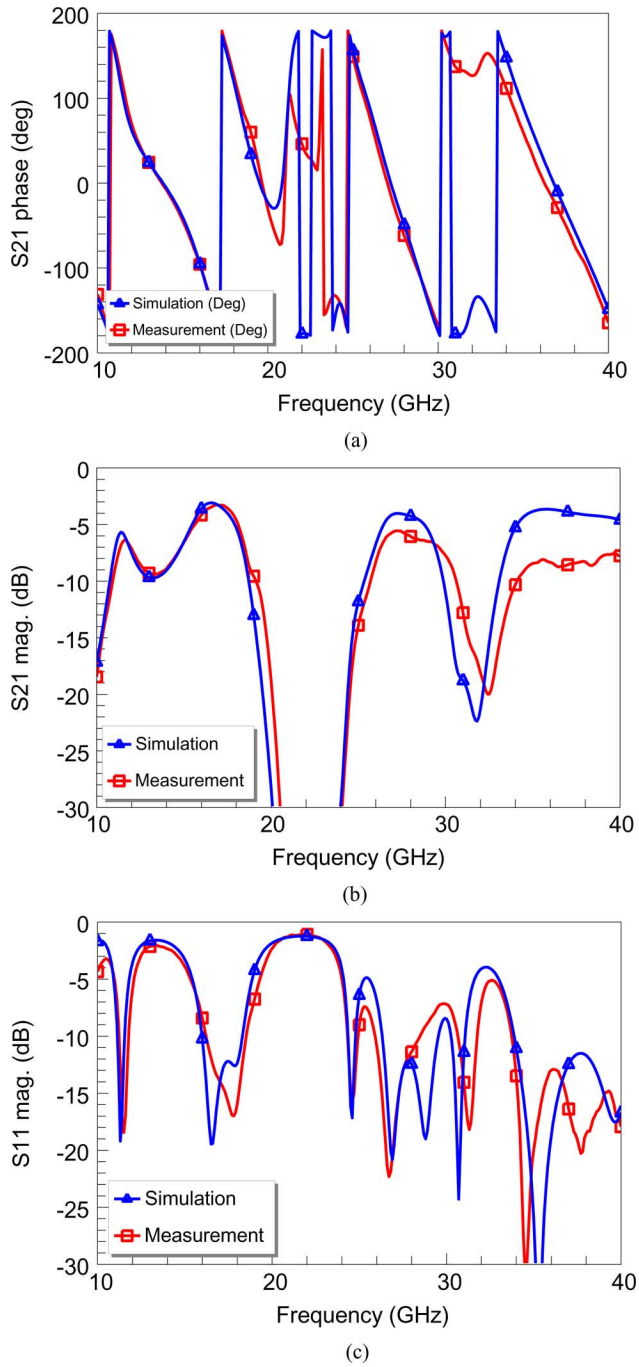

Fig. 14. Measurement results of the RF MEMS phase shifter when it is to 180° insertion phase state at 40 GHz compared with the simulations (operation state: 180, 40 GHz). (a) S_{21} phase. (b)$|S_{21}|$. (c) $|S_{11}|$. This figure shows that the measurement results are still in agreement with the simulations within the whole 10–40-GHz band once it is set to a specific state at a given frequency.

are no steps on the MEMS bridges. A proof for this statement is that the MAM capacitances, which are also parts of the phase shifter, are totally flat; their bridge heights are measured exactly as expected. However, because of the weak junction points, the bridge height of the MEMS switch is decreased, and as a result, C_{bu} increases. The change in C_{bu} also changes the insertion phases of all of the DMTL unit sections, and the phase shift decreases about 1°–2° per unit section. The effects of the increase of C_{bu} on the performance of the phase shifter will be

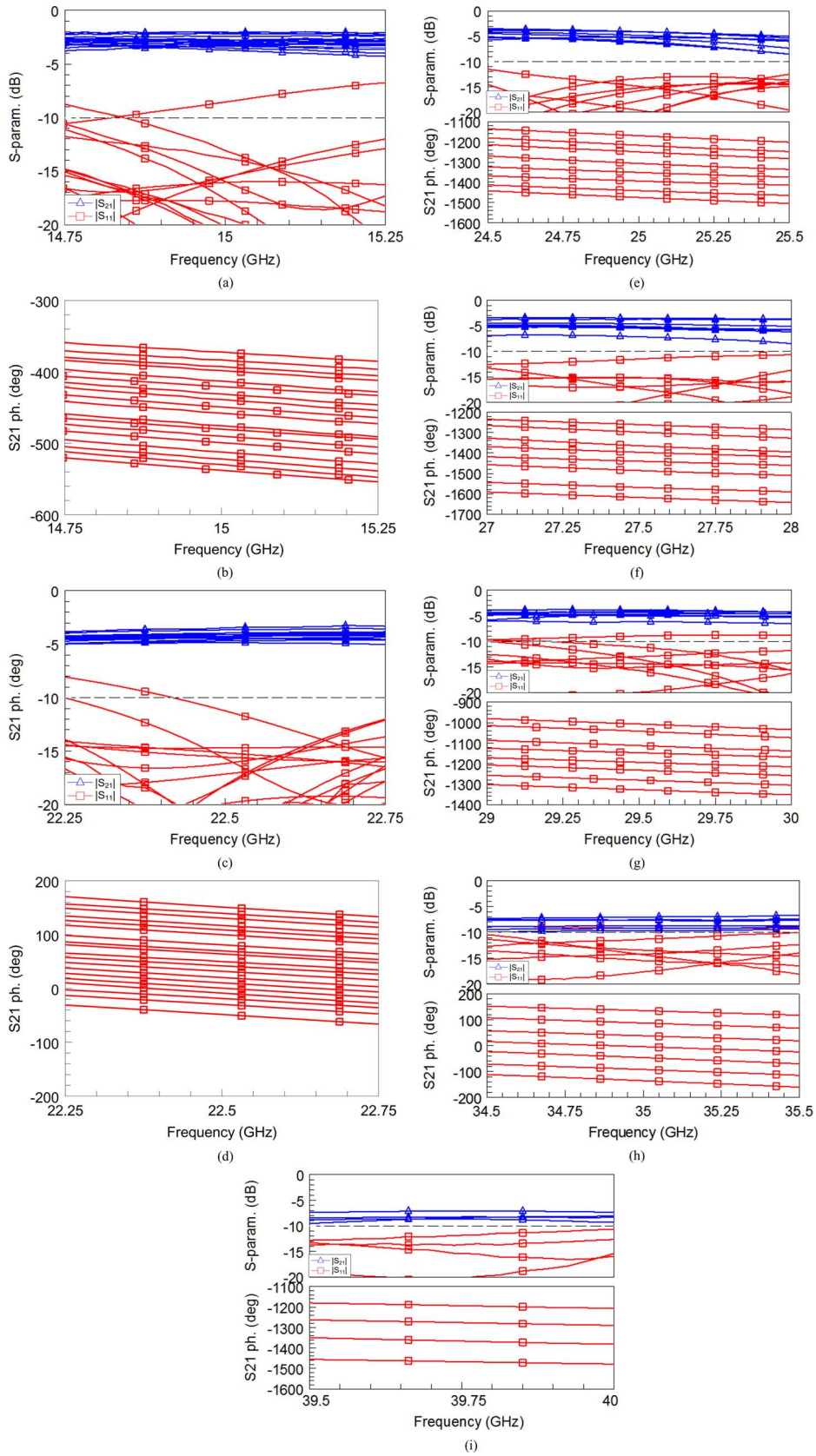

Fig. 15. Measurement results of the RF MEMS phase shifter when it is reconfigured at sample frequencies in 15–40-GHz band. (a) 15-GHz insertion loss and return loss. (b) 15-GHz insertion phase. (c) 22.5-GHz insertion loss and return loss. (d) 22.5-GHz insertion phase. (e) 25 GHz. (f) 27.5 GHz. (g) 30 GHz. (h) 35 GHz. (i) 40 GHz.

discussed in Section IV-C. The value of biasing resistors, R_{bias}, also show some difference between the measured and simulated values. The values presented above are actually the RF resistors values, which cannot be extracted independently from mea-

TABLE IV
SUMMARY OF THE RF MEMS PHASE-SHIFTER MEASUREMENT RESULTS

Frequency (GHz)	Phase Range (°)	Resolution (°)	Number of Meas. States	Avg. IL (dB)	Avg. RL (dB)	Avg. Phase Err. (°)
15	0-180	10	19	3.0	19.3	1.6
22.5	0-180	10	19	4.2	20.7	1.0
25	0-360	45	8	5.0	17.3	7.3
27.5	0-315	45	7	5.0	17.5	4.4
30	0-360	45	8	5.0	15.8	3.7
35	0-315	45	7	8.2	13.7	2.1
40	0-360	90	4	8.2	13.7	4.7

surements and are affected from the values of other components that generate losses. The simulated and measured values are extracted from HFSS simulations and DMTL measurements, respectively, which give the best fit with the circuit model and both result different values than their dc values.

C. Phase-Shifter Measurements

The measurements of the RF MEMS phase shifter are made using the MAMS, and the same parameters that were explained above are used during the measurements. Fig. 14 presents the measurement results of the RF MEMS phase shifter when it is set to 180° insertion phase state at 40 GHz as a sample, and the results are compared with the simulations. The graphs show that when the phase shifter is set to this sample state, its performance at 40 GHz is good as expected, and the measurement results are still in agreement with the simulations within the whole targeted 10–40-GHz band.

In order to demonstrate the frequency reconfigurable phase shifting capability of the presented design, the RF MEMS phase shifter is configured to work at some sample frequencies between 15–40 GHz. For any desired phase state at any selected sample frequency, first the required electrical lengths for the connecting transmission lines and stubs are determined for the desired insertion phase state using the theory explained in Section II. The states of the connecting transmission lines and stubs are then configured to give those electrical lengths, and the desired insertion phase is obtained at the selected sample frequency. A reference insertion phase state is also selected at each frequency for the phase-shift calculations. The measurement results are presented in Fig. 15 where the phase shifter is set to work at 15, 22.5, 25, 27.5, 30, 35, and 40 GHz.

For the 15–22.5-GHz band, the phase shifter is measured at two sample frequencies, which are 15 and 22.5 GHz, and the phase shifter is set for 10° phase steps in the 0°–180° range. For the 22.5–30-GHz band, the phase shifter is measured at three sample frequencies, which are 25, 27.5, and 30 GHz, and the phase shifter is set for 45° phase steps. For the 30–40-GHz band, the phase shifter is measured at two sample frequencies, which are 35 and 40 GHz, and the phase shifter is set for 45° and 90° phase steps, respectively. These measurement results, which are presented in Fig. 15, on these randomly picked frequencies clearly show that the presented phase shifter is capable of operating at any frequency within the aforementioned band. Table IV summarizes the measurement results at all frequencies.

The measurement results are presented in the 0°–180° range instead of the 0°–360° range at 15 GHz. This is a result of the decrease in the gap between the MEMS bridge and CPW. This strongly reduces the up/down capacitance ratio in all three types of DMTL unit sections. As a result, the insertion phase for each unit section type is different, and the phase shift per unit section is affected significantly. This situation not only changes the up-state insertion phase of connecting transmission lines and stubs, but also decreases the phase shift that can be inserted by them. These two parameters are both critical for the operation of the phase shifter and alter its operation as a natural result of the theory of the triple-stub circuit topology, as explained previously in Section II and shown in Fig. 2. It should be noted here that the phase shifter can actually provide 0°–360° phase shift at 15 GHz even with the given up/down ratio, but the insertion losses start to increase significantly after some point. The maximum phase range with acceptable insertion loss increases naturally as the operation frequency is increased. The reader is kindly asked to refer to [20] for further details of the theory. Nevertheless, thanks to the flexibility of the triple-stub topology and reconfigurability of the design, the fabricated phase shifter is still operational within the whole targeted band.

Considering the results presented in Table IV, different phase resolutions and ranges are observed for different frequencies. As explained previously in Section II, the phase shifter was designed for 10° phase resolution with a range of 0°–360° at the minimum frequency of the band of interest, 15 GHz. The DMTL unit sections were designed with minimal insertion phases and phase shifts that satisfy the design requirements at this frequency. However, as the operation frequency increases, the insertion phase and phase shift per unit section also increases naturally, which increases the minimum step size of the connecting transmission lines and stubs, and the phase resolution of the phase shifter increases accordingly. The same situation is also true for the phase range. The phase range at 15 GHz, which was reduced due to the decrease in the up/down capacitance ratio of the MEMS switch, also increases as the electrical lengths of the connecting transmission lines and stubs increase as explained above. The limit for the phase resolution is the limit at the minimum frequency of the band.

The loss performance of the fabricated phase shifter is measured to be slightly higher than the simulated values in 15–30-GHz band. The reason for this is mainly due to the change in the gap between the MEMS bridge and CPW in all unit section types. As reported in [13], [15], and [26], the losses per unit section in a loaded line are given in (1) and (2) as follows:

$$\alpha_{ld,u} \cong \frac{R_t}{2Z_{lu}} + \frac{R_s Z_{lu} \omega^2 C_{bu}^2}{2} \text{ Np/unit section} \quad (1)$$

$$\alpha_{ld,d} \cong \frac{R_t}{2Z_{ld}} + \frac{Z_{ld}}{2R_p} \text{ Np/unit section} \quad (2)$$

TABLE V
COMPARISON OF STATE-OF-THE-ART PHASE SHIFTERS

Type	Frequency (GHz)	Phase Range (°)	Resolution (°)	Avg. IL (dB)	Avg. RL (dB)	Avg. Phase Error (°)
Low-pass/high-pass, BiCMOS, 2008, [28]	35 (31-38)	0-360	22.5	-13	< -10 dB	11
Quadrature all-pass, CMOS, 2007, [29]	15-26	0-360	22.5	-3.8	< -10 dB	9.7
DMTL, MEMS, 2012, [30]	15	0-360	22.5	-1.7	< -10 dB	7
DMTL, MEMS, 2012, [30]	35	0-360	22.5	-2.7	< -13 dB	6.7
Switched line, MEMS, 2003, [10]	35 (0-40)	0-360	45	-2.2	< -15 dB	2.3
Reflection type, MEMS, 2003, [31]	15-45	0-40	10	-3.5	< -10 dB	4.9
This work	15-40	0-180 @ 15-25 GHz 0-315 @ 22.5-40 GHz	10 @ 15-25 GHz 45 @ 22.5-35 GHz 90 @ 35-40 GHz	-3.6 @ 15-22.5 GHz -5 @ 25-30 GHz -8.2 @ 35-40 GHz	< -19 @ 15-22.5 GHz < -16 @ 25-30 GHz -13.7 @ 35-40 GHz	1.3 @ 15-22.5 GHz 5.2 @ 25-30 GHz 3.4 @ 35-40 GHz

where R_t is the unloaded CPW resistance, and R_s and R_p is the total series and parallel resistances in the up-state and down-state, respectively. The decrease in the gap increases C_{bu} and decreases Z_{lu}, both of which increase loss per unit section in the up-state. The bridge resistance, R_b, is also extracted higher than the simulated value because of the high resistivity of the electroplated gold. All three effects increase the loss of the DMTL unit sections by 20% and 38% at 15 and 30 GHz, respectively. It should be noted here that, in any operation state of the phase shifter, there are many unit sections that are in the up-state. Moreover, the phase shifter is a resonant type circuit so the increase in the loss of the DMTL unit sections causes a nonlinear increase on the total loss of the phase shifter.

For the 30–40-GHz band, another loss factor becomes important, which is the radiation loss for the CPW. According the formulation presented in [27], the radiation losses for the CPW that is used in the phase shifter are 1.3, 10.4, and 24.7 dB/m for 15, 30, and 40 GHz, respectively. These values are 3.7%, 21%, and 44% of the conductor losses at the corresponding frequencies, which means that the radiation losses become comparably significant after 30 GHz. This explains the increasing loss behavior of the phase shifter in the 30–40-GHz band. The radiation loss above 30 GHz can be reduced significantly by decreasing gap, G, of the CPWs while keeping the $W/(W+2G)$ ratio the same (Fig. 4).

Table V gives a comparison of the proposed phased shifter with state-of-the-art phase shifters.

V. CONCLUSION

A wideband frequency reconfigurable adjustable phase step RF MEMS phase shifter has been presented. The presented design is capable of operating *at any frequency* within the 15–40-GHz band *with adjustable phase steps* using the advantages of the triple-stub topology and MEMS technology. The design can be easily scaled to work at lower or higher frequency bands and optimized to work for wider frequency bands. The authors strongly believe that the loss performance can also be improved considerably by optimizing the number and the position of the DMTL unit sections and the number of resistive bias lines used in the design.

Finally, it should be noted here that this study only makes a demonstration of the frequency reconfigurable phase shifting with adjustable phase steps using triple-stub topology. No specific effort was spent in order to optimize the performance of the phase shifter or to minimize the number of control pins. The authors strongly believe that the number of control pins can be reduced significantly for different designs that have different phase resolution and bandwidth requirements, which makes the design more feasible for applications that employ a high number of phase shifters. In addition to that, the presented phase shifter can also be realized with four control signals provided that the electrical length requirements for the connecting transmission lines and stubs are satisfied. The presented phase shifter can also be implemented using other state-of-the-art fabrication technologies and is a very strong candidate for wideband multi-frequency systems where it can replace multiple phase shifters and decrease the system complexity significantly.

ACKNOWLEDGMENT

The authors would like to thank O. Akar for his valuable guidance during the fabrication, H. Ibrahim Atasoy, C. Cetintepe, Dr. K. Topalli, and C. Berry for their help. The authors would also would like to thank the METU-MEMS Center, Ankara, Turkey, personnel for their support.

REFERENCES

[1] B. M. Schiffman, "A new class of broadband microwave 90-degree phase shifters," *IRE Trans. Microw. Theory Techn.*, vol. MTT-6, no. 2, pp. 232–237, Apr. 1958.

[2] R. V. Garver, "Broad-band diode phase shifters," *IEEE Trans. Microw. Theory Techn.*, vol. MTT-20, no. 5, pp. 297–304, May 1972.

[3] D. Adler and R. Popovich, "Broadband switched-bit phase shifter using all-pass networks," presented at the IEEE MTT-S Int. Microw. Symp., Boston, MA, USA, Jun. 1991.

[4] E. G. Erker, A. S. Nagra, L. Yu, P. Periaswamy, T. R. Taylor, J. Speck, and R. A. York, "Monolithic Ka-band phase shifter using voltage tunable BaSrTiO3 parallel plate capacitors," *IEEE Microw. Guided Wave Lett.*, vol. 10, no. 1, pp. 10–12, Jan. 2000.

[5] K. Hongjoon, A. B. Kozyrev, A. Karbassi, and D. W. Van Der Weide, "Linear tunable phase shifter using a left-handed transmission line," *IEEE Microw. Wireless Compon. Lett.*, vol. 15, no. 5, pp. 366–368, May 2005.
[6] F. De Flaviis, N. G. Alexopoulos, and O. M. Stafsudd, "Planar microwave integrated phase-shifter design with high purity ferroelectric material," *IEEE Trans. Microw. Theory Techn.*, vol. 45, no. 6, pp. 963–969, Jun. 1997.
[7] C. Qingjiang, Q. Li, Z. Ziyang, Q. Min, Y. Tong, and S. Yikai, "A tunable broadband photonic RF phase shifter based on a silicon microring resonator," *IEEE Photon. Technol. Lett.*, vol. 21, no. 1, pp. 60–62, Jan. 2009.
[8] S. Muller, P. Scheele, C. Weil, M. Wittek, C. Hock, and R. Jakoby, "Tunable passive phase shifter for microwave applications using highly anisotropic liquid crystals," in *IEEE MTT-S Int. Microw. Symp. Dig.*, Fort Worth, TX, USA, Jun. 2004, pp. 1153–1156.
[9] G. L. Tan, R. E. Mihailovich, J. B. Hacker, J. F. DeNatale, and G. M. Rebeiz, "Low-loss 2- and 4-bit TTD MEMS phase shifters based on SP4T switches," *IEEE Trans. Microw. Theory Techn.*, vol. 51, no. 1, pp. 297–304, Jan. 2003.
[10] J. B. Hacker, R. E. Mihailovich, M. Kim, and J. F. DeNatale, "A Ka-band 3-bit RF MEMS true-time-delay network," *IEEE Trans. Microw. Theory Techn.*, vol. 51, no. 1, pp. 305–308, Jan. 2003.
[11] B. Pillans, S. Eshelman, A. Malczewski, J. Ehmke, and C. Goldsmith, "Ka-band RF MEMS phase shifters," *IEEE Microw. Guided Wave Lett.*, vol. 9, no. 12, pp. 520–522, Dec. 1999.
[12] G. L. Tan, R. E. Mihailovich, J. B. Hacker, J. F. DeNatale, and G. M. Rebeiz, "A 4-bit miniature X-band MEMS phase shifter using switched-LC networks," in *IEEE MTT-S Int. Microw. Symp. Dig.*, Philadelphia, PA, USA, Jun. 2003, pp. 1477–1480.
[13] N. S. Barker and G. M. Rebeiz, "Optimization of distributed MEMS transmission-line phase shifters—U-band and W-band design," *IEEE Trans. Microw. Theory Techn.*, vol. 48, no. 11, pp. 1957–1966, Nov. 2000.
[14] Y. Liu, A. Borgioli, A. S. Nagra, and R. A. York, "K-band 3-bit low-loss distributed MEMS phase shifter," *IEEE Microw. Guided Wave Lett.*, vol. 10, no. 10, pp. 415–417, Oct. 2000.
[15] J. S. Hayden and G. M. Rebeiz, "Very low loss distributed X-band and Ka-band MEMS phase shifters using metal–air–metal capacitors," *IEEE Trans. Microw. Theory Techn.*, vol. 51, no. 1, pp. 309–314, Jan. 2003.
[16] J.-J. Hung, L. Dussopt, and G. M. Rebeiz, "Distributed 2- and 3-bit W-band MEMS phase shifters on glass substrates," *IEEE Trans. Microw. Theory Techn.*, vol. 52, no. 2, pp. 600–606, Feb. 2004.
[17] T. Vähä-Heikkilä, J. Varis, J. Tuovinen, and G. M. Rebeiz, "W-band RF MEMS double and triple-stub impedance tuners," in *IEEE MTT-S Int. Microw. Symp. Dig.*, Long Beach, CA, USA, Jun. 2005, pp. 12–17.
[18] M. Unlu, K. Topalli, H. I. Atasoy, E. U. Temocin, I. Istanbulluoglu, O. Bayraktar, S. Demir, O. A. Civi, S. Koc, and T. Akin, "A reconfigurable RF MEMS triple stub impedance matching network," in *Proc. 36th Eur. Microw. Conf.*, Manchester, U.K., Sep. 2006, pp. 1370–1373.
[19] T. Vähä-Heikkilä, K. Van Caekenberghe, J. Varis, J. Tuovinen, and G. M. Rebeiz, "RF MEMS impedance tuners for 6–24 GHz applications," *Int. J. RF Microw. Comput.-Aided Eng.*, vol. 17, no. 3, pp. 265–278, May 2007.
[20] M. Unlu, S. Demir, and T. Akin, "Triple stub circuit topology as simultaneous insertion phase, amplitude, and impedance control circuit for phased array applications," *IET Microw. Antennas Propag*, vol. 6, no. 13, pp. 1399–1406, Dec. 2012.
[21] M. Unlu, "Novel impedance tuner, phase shifter, and vector modulators using RF MEMS technology," Ph.D. dissertation, Dept. Elect. Electron. Eng., Middle East Techn. Univ., Ankara, Turkey, 2009.
[22] HFSS. ver. 10, Ansoft Corporation, Pittsburgh, PA, USA, 2002.
[23] AWR Microwave Office 2006. Appl. Wave Res. Inc., El Segundo, CA, USA, 2006.
[24] K. Topalli, O. Aydin Civi, S. Demir, S. Koc, and T. Akin, "A monolithic phased array using 3-bit distributed RF MEMS phase shifters," *IEEE Trans. Antennas Propag.*, vol. 56, no. 2, pp. 270–277, Feb. 2008.
[25] O. D. Gurbuz, "Reliability improvement of RF MEMS devices based on lifetime measurements," M.Sc. thesis, Dept. Elect. Electron. Eng., Middle East Technical Univ., Ankara, Turkey, 2010.
[26] M. J. W. Rodwell, S. T. Allen, R. Y. Yu, M. G. Case, U. Bhattacharya, M. Reddy, E. Carman, M. Kamegawa, Y. Konishi, J. Pusl, and R. Pullela, "Active and nonlinear wave propagation devices in ultrafast electronics and optoelectronics," *Proc. IEEE*, vol. 82, no. 7, pp. 1037–1059, Jul. 1994.
[27] D. B. Rutledge, D. P. Neikirk, and D. P. Kasilingam, "Infrared and Millimeter Waves," in *Integrated-Circuit Antennas*, K. J. Button, Ed. New York, NY, USA: Academic, 1983, vol. 10, ch. 1.
[28] B. Min and G. M. Rebeiz, "Single-ended and differential Ka-band BiCMOS phased array front-ends," *IEEE J. Solid-State Circuits*, vol. 43, no. 10, pp. 2239–2250, Oct. 2008.
[29] K. Kwang-Jin and G. M. Rebeiz, "0.13-μm CMOS phase shifters for X-, Ku-, and K-band phased arrays," *IEEE J. Solid-State Circuits*, vol. 42, no. 11, pp. 2535–2546, Nov. 2007.
[30] B. Pillans, L. Coryell, A. Malczewski, C. Moody, F. Morris, and A. Brown, "Advances in RF MEMS phase shifters from 15 GHz to 35 GHz," in *IEEE MTT-S Int. Microw. Symp. Dig.*, Montreal, QC, Canada, Jun. 2012, pp. 1–3.
[31] S. Lee, J.-H. Park, H.-T. Kim, J.-M. Kim, Y.-K. Kim, and Y. Kwon, "Low-loss analog and digital reflection-type MEMS phase shifters with 1:3 bandwidth," *IEEE Trans. Microw. Theory Techn.*, vol. 52, no. 1, pp. 211–219, Jan. 2004.

Mehmet Unlu (S'00–M'11) received the B.S., M.S., and Ph.D. degrees in electrical and electronics engineering from Middle East Technical University (METU), Ankara, Turkey, in 2001, 2003, and 2009, respectively.

In 2009, he was Postdoctoral Researcher with the Middle East Technical University Microelectromechanical Systems (METU-MEMS) Center, Ankara, Turkey. From 2010 to 2011, he was a Research Scientist with Utah State University, Logan, UT, USA, while he conducted his research activities with the Cornell Nanoscale Science and Technology Facility (CNF), Ithaca, NY, USA. From 2011 to 2012, he was also a Postdoctoral Research Fellow with the Terahertz Electronics Laboratory, Electrical and Electronic Computer Science Department, The University of Michigan at Ann Arbor. Since 2012, he has been an Assistant Professor with Yildirim Beyazit University, Ankara, Turkey. He has authored/coauthored over 30 peer-reviewed academic journals and conference papers. His major research interests are terahertz electronics, RF MEMS, and reconfigurable circuits and antennas for microwave, and millimeter-wave applications.

Dr. Unlu was the recipient of the 2009 METU Thesis of the Year Award for his Ph.D. dissertation, which was awarded by the Prof. Mustafa N. Parlar Education and Research Foundation. He was also the recipient of a graduate fellowship presented by the Scientific and Technical Research Council of Turkey (TUBITAK).

Simsek Demir (S'91–M'98) received the B.Sc., M.Sc., and Ph.D. degrees in electrical and electronics engineering from Middle East Technical University (METU), Ankara, Turkey, in 1991, 1993 and 1998, respectively.

From 1991 to 1998, he was a Research Assistant with METU. From 1998 to 1999, he contributed to atmospheric radar antenna design with the International Research Centre for Telecommunications and Radar (IRCTR), Technical University of Delft (TU-Delft), Delft, The Netherlands. Since 2000, he has been a Professor with the Electrical and Electronics Engineering Department, METU. His scientific interests include microwave and millimeter-wave active and passive component and system design, analysis, and modeling. Exploitation of RF MEMS technology toward industrial use, power amplifier design, modeling and implementation, and radar applications are some of his particular research topics.

Dr. Demir was a recipient of several awards, including North American Treaty Organization (NATO) A2 Fellowship, which supported him as a Visiting Researcher with the University of Massachusetts at Amherst, in 1995.

Tayfun Akin (S'90–M'97) was born in Van, Turkey, in 1966. He received the B.S. degree in electrical engineering (with high honors) from Middle East Technical University, Ankara, Turkey, in 1987, and the M.S. and Ph.D. degrees in electrical engineering, from The University of Michigan at Ann Arbor, Ann Arbor, MI, USA, in 1987 and 1994, respectively.

Since 1995, 1998, and 2004, he has been an Assistant Professor, Associate Professor, and Professor, respectively, with the Department of Electrical and Electronics Engineering, Middle East Technical University (METU), Ankara, Turkey. He is also the Director of the Middle East Technical University Microelectromechanical Systems (METU-MEMS) Center, Ankara, Turkey, which has a 1300-m^2 clean-room area for MEMS process and testing. His research interests include MEMS, microsystems technologies, infrared detectors and readout circuits, silicon-based integrated sensors and transducers, and analog and digital integrated circuit design.

Dr. Akin has served on various MEMS, Eurosensors, and Transducers conferences as a Technical Program Committee member. He was the cochair of the 19th IEEE International Conference of Micro Electro Mechanical Systems (MEMS 2006), Istanbul, Turkey. He was the cochair of the Steering Committee, IEEE MEMS Conference, in 2007. He was the recipient of a graduate fellowship from the North American Treaty Organization (NATO) Science Scholarship Program through the Scientific and Technical Research Council of Turkey (TUBITAK) in 1987. He was also the recipient of the First Prize in Experienced Analog/Digital Mixed-Signal Design Category of the 1994 Student Very Large Scale Integration (VLSI) Circuit Design Contest organized and sponsored by Mentor Graphics, Texas Instruments Incorporated, Hewlett-Packard, Sun Microsystems, and *Electronic Design Magazine*. He coauthored the symmetric and decoupled gyroscope project, which won the First Prize Award of the Operational Designs Category of the International Design Contest organized by the DATE Conference and CMP in 2001. He also coauthored the gyroscope project, which won the Third Prize Award of the 3-D MEMS Design Challenge organized by MEMGen Corporation (currently Microfabrica).